



저작자표시-비영리-변경금지 2.0 대한민국

이용자는 아래의 조건을 따르는 경우에 한하여 자유롭게

- 이 저작물을 복제, 배포, 전송, 전시, 공연 및 방송할 수 있습니다.

다음과 같은 조건을 따라야 합니다:



저작자표시. 귀하는 원저작자를 표시하여야 합니다.



비영리. 귀하는 이 저작물을 영리 목적으로 이용할 수 없습니다.



변경금지. 귀하는 이 저작물을 개작, 변형 또는 가공할 수 없습니다.

- 귀하는, 이 저작물의 재이용이나 배포의 경우, 이 저작물에 적용된 이용허락조건을 명확하게 나타내어야 합니다.
- 저작권자로부터 별도의 허가를 받으면 이러한 조건들은 적용되지 않습니다.

저작권법에 따른 이용자의 권리는 위의 내용에 의하여 영향을 받지 않습니다.

이것은 [이용허락규약\(Legal Code\)](#)을 이해하기 쉽게 요약한 것입니다.

[Disclaimer](#)

Master's Thesis  
석사 학위논문

# Band-Gap Tunable Colloidal Perovskite Nanocrystals Functionalized with Formamidinium Cations for Photodetector Application

Tatachari Santhanagopalan Shridharan  
Department of  
Energy Science & Engineering

DGIST

2020

Master's Thesis  
석사 학위논문

# Band-Gap Tunable Colloidal Perovskite Nanocrystals Functionalized with Formamidinium Cations for Photodetector Application

Tatachari Santhanagopalan Shridharan  
Department of  
Energy Science & Engineering

DGIST

2020

# Band-Gap Tunable Colloidal Perovskite Nanocrystals Functionalized with Formamidinium Cations for Photodetector Application

Advisor: Professor Jong-Soo Lee

Co-advisor: Dr. Younghoon Kim

by

Tatachari Santhanagopalan Shridharan

Department of Energy Science & Engineering

DGIST

A thesis submitted to the faculty of DGIST in partial fulfillment of the requirements for the degree of Master of Science in the Department of Energy Science & Engineering. The study was conducted in accordance with the Code of Research Ethics<sup>1</sup>

2019.11.08

Approved by

Professor Jong-Soo Lee  
(Advisor)



(signature)

Dr. Younghoon Kim  
(Co-Advisor)



(signature)

---

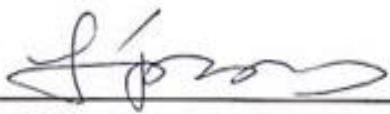
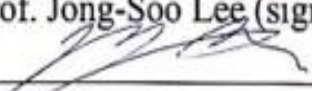
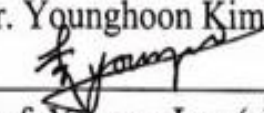
<sup>1</sup> Declaration of Ethical Conduct in Research: I, as a graduate student of DGIST, hereby declare that I have not committed any acts that may damage the credibility of my research. These include, but are not limited to: falsification, thesis written by someone else, distortion of research findings or plagiarism. I affirm that my thesis contains honest conclusions based on my own careful research under the guidance of my thesis advisor.

# Band-Gap Tunable Colloidal Perovskite Nanocrystals Functionalized with Formamidinium Cations for Photodetector Application

Tatachari Santhanagopalan Shridharan

Accepted in partial fulfillment of the requirements for the degree of Master of Science.

2019.11.08

Head of Committee	 Prof. Jong-Soo Lee (signature)
Committee Member	 Dr. Younghoon Kim (signature)
Committee Member	 Prof. Youngu Lee (signature)

MS/ES  
201824003

Tatachari Santhanagopalan Shridharan. Band-Gap Tunable Colloidal Perovskite Nanocrystals Functionalized with Formamidinium Cations for Photodetector Application. Department of Energy Science & Engineering 2020. 39p. Advisors Prof. Jong-Soo Lee, Co-Advisors Dr. Younghoon Kim

## ABSTRACT

Colloidal quantum dots of lead halide perovskites (PQDs) have drawn much attention in the field of various optoelectronic applications such as solar cells, lasers and light emitting diodes (LEDs) due to their size- and composition-dependent optical bandgaps ( $E_g$ ), high absorption coefficient, defect tolerance band structure and narrow band emission. Various PQDs such as  $\text{CsPbI}_3$ ,  $\text{FAPbI}_3$ , and  $\text{Cs}_{1-x}\text{FA}_x\text{PbI}_3$  have been largely used as a photovoltaic absorber in room-temperature and solution-processed thin film solar cells because of the use of pre-crystallized PQDs while fabricating the PQD thin films, which lead to the absence of thermal annealing process normally used in conventional perovskite thin film approach. For analysing the charge transport properties, the PQDs could be employed on photodetectors. Because of low trap density, long carrier life time and diffusion length, PQDs are an ideal material to improve the performance of the photodetectors. PQDs are used a semiconducting material in the photodetector which absorbs the incident photon and generate the electron-hole pair. Photocurrent is generated as result of extraction of the charge carries with the application of external or build-in electric field. In particular, transistor-type photodetector is used, as the photoresponsivity of the material increases without the loss of response speed. During the operation of the device, the high mobility of the material is obtained through the accumulation of charge carriers across the channel. Also, due to the reduced recombination rate of the photogenerated electron-hole pair, the carrier life time is increased.

In this work, we introduce a strategy to improve the inherent charge transporting of the PQDs thin film by selective removal of anionic oleates and cationic oleylammonium. First, to study on the optical properties of the PQDs,  $\text{CsPbI}_3$  and  $\text{FAPbI}_3$  are synthesised through hot injection method. The A-site interplay between the  $\text{CsPbI}_3$  and  $\text{FAPbI}_3$  leads to the formation of  $\text{Cs}_{1-x}\text{FA}_x\text{PbI}_3$  through controlled cation exchange reaction. Also, since the amount of ligands bound to each PQDs varies after the synthesis, the removal and replacement of the surface passivating long chain ligands with a short chain ligand through ligand exchange mechanism improves the coupling between the quantum dots. Furthermore, to study the inherent charge transport mechanism, incorporating the PQDs in transistor-type photodetector lead to many significant observations.

Keywords: PQDs, Cation Exchange, Anion Exchange, Inherent charge transferring.

# List of Contents

Abstract .....	v
List of contents .....	vi-vii
List of figures .....	viii
<b>I. Part -1 – Synthesis of Bandgap Tunable Perovskite Quantum Dots</b>	
<b>1 - Introduction</b> .....	2
1.1 Perovskite Crystal Structure .....	2
1.2 Solution Processing of Perovskites .....	4
<b>2 – Experimental Section</b> .....	9
2.1 Synthesis of Cs-Oleate Precursor .....	9
2.2 Synthesis of FA-Oleate Precursor .....	9
2.3 Synthesis of CsPbI <sub>3</sub> .....	10
2.4 Synthesis of FAPbI <sub>3</sub> .....	11
2.5 Synthesis of FA <sub>1-x</sub> Cs <sub>x</sub> PbI <sub>3</sub> .....	12
<b>3 – Characterization</b> .....	13
3.1 UV-Vis Spectroscopy .....	13
3.2 Photoluminescence spectroscopy .....	13
3.3 TRPL spectroscopy .....	13
3.4 X-Ray Diffraction .....	13
3.5 Transmission Electron microscopy .....	13
3.6 FTIR spectroscopy .....	14
<b>4 – Results and Discussion</b> .....	15
<b>II. Part -2 – Application of PQDs in Photodetector</b>	
<b>1 - Introduction</b> .....	25
<b>2 – Device Fabrication</b> .....	28
<b>3 – Results and Discussion</b> .....	30
<b>4 – Conclusion</b> .....	30

<b>References</b> .....	35
<b>Figure 1.</b> NREL Solar Cell Efficiency Chart .....	3
<b>Figure 2.</b> Perovskite crystal structure .....	4
<b>Figure 3.</b> Goldschmidt tolerance factor for perovskites cations .....	5
<b>Figure 4.</b> Schematic representation of the synthesis of CsPbI <sub>3</sub> .....	10
<b>Figure 5.</b> Schematic representation of the synthesis of FAPbI <sub>3</sub> .....	11
<b>Figure 6.</b> Transmission electron microscopy images of (a) CsPbI <sub>3</sub> (b) Cs <sub>1-x</sub> FA <sub>x</sub> PbI <sub>3</sub> (c)FAPbI <sub>3</sub> nanocrystals and (d) Photoluminescence of the solution samples. Inset figure shows the HRTEM of single nanocrystal .....	16
<b>Figure 7.</b> Schematic representation of removal of long chain oleic acid and oleylamonium lig-and and incorporation of FA+ cations .....	18
<b>Figure 8:</b> Shifting of PL peaks in the process of ligand exchange (a) CsPbI <sub>3</sub> (b) FA <sub>1-x</sub> Cs <sub>x</sub> PbI <sub>3</sub> (c)FAPbI <sub>3</sub> nanocrystals and (d) Summarized chart representing the peak position shift. ....	19
<b>Figure 9.</b> FTIR spectroscopy of pristine and ligand exchanged samples of the PQD film .....	20
<b>Figure 10.</b> Time resolved spectroscopy of pristine and ligand exchanged samples of the PQD film .....	21
<b>Figure 11.</b> Representation of types of photodetectors .....	24
<b>Figure 12.</b> Perovskite-based FET device .....	26
<b>Figure 13.</b> Ligand Exchnage process of PQDs .....	27
<b>Figure 14.</b> (a)I-V characteristics of CsPbI <sub>3</sub> as a function of incident light intensity. (b) Dependence of responsivity and detectivity on incident power of CsPbI <sub>3</sub> photodetector measured at V <sub>ds</sub> = 5V and V <sub>g</sub> = 0V. (c) Photocurrent-Time (I <sub>ph-t</sub> ) response measured in dark and under illumination using a laser source at 405nm. (d) Time resolved analysis of rise and decay time @42.6W/cm <sup>2</sup> . ....	29
<b>Figure 15.</b> (a)I-V characteristics of FA <sub>1-x</sub> Cs <sub>x</sub> PbI <sub>3</sub> as a function of incident light intensity. (b) Dependence of responsivity and detectivity on incident power of FA <sub>1-x</sub> Cs <sub>x</sub> PbI <sub>3</sub> photodetector measured at V <sub>ds</sub> = 5V and V <sub>g</sub> = 0V. (c) Photocurrent-Time (I <sub>ph-t</sub> ) response measured in dark and under illumination using a laser source at 405nm. (d) Time resolved analysis of rise and decay time @42.6W/cm <sup>2</sup> . .	30



**Figure 16.** (a) I-V characteristics of FAPbI<sub>3</sub> as a function of incident light intensity. (b) Dependence of responsivity and detectivity on incident power of FAPbI<sub>3</sub> photodetector measured at V<sub>ds</sub> = 5V and V<sub>g</sub> = 0V. (c) Photocurrent-Time (I<sub>ph-t</sub>) response measured in dark and under illumination using a laser source at 405nm. (d) Time resolved analysis of rise and decay time @42.6W/cm<sup>2</sup>. ..... 32

# **PART 1**

## **Synthesis of band-gap tunable perovskite Quantum dots**

# 1. INTRODUCTION

Looking over the energy demand, the world is encountered by non-sustainable resources which include coal, oil and natural gas. So, alternative for these is the renewable resources which mainly include solar energy. But, replacing the existing silicon wafer technology with an energy conversion is crucial for obtaining economic solar technology. In the recent decades, the lead halide perovskites (LHP's) have drawn much attention in the field of optoelectronic devices like light-emitting devices and photodetectors due to their tunable color wavelength, high electron/hole mobility, strong light absorption coefficients, defect tolerance, narrowband emission, and electrical properties. Apart from these properties, they can be easily synthesized through solution processing and the cost of the fabrication is less, which makes it an important candidate for optoelectronic devices <sup>[1,2]</sup>. Due to the prospect of size controllability and quantum size effects, these perovskite nanocrystals (NC's) in the form of quantum dots have been adopted for the photovoltaic and optoelectronic application <sup>[3]</sup>.

## 1.1 Perovskite Crystal Structure

The main material of interest exhibits the  $ABX_3$  structured perovskites (where A and B represent the organic-inorganic cation and Pb respectively and X is the halide anion) which includes the inorganic LHP's, i.e.,  $CsPbI_3$  and the hybrid organic-inorganic LHP's, i.e.,  $MAPbI_3$  (MA:  $CH_3NH_3^+$  - Methylammonium) and  $FAPbI_3$  (FA:  $CH(NH_2)_2^+$  - Formamidinium). These materials can be tuned in the ultraviolet to near infra-red range based on the cationic ratios (for FA-Cs) and halide compositions or crystal size of the perovskites based on the synthesis

[4]. The lattice structure and the photoconductivity of the perovskite materials especially  $\text{CsPbI}_3$  were reported late back in the early 1950s [5].

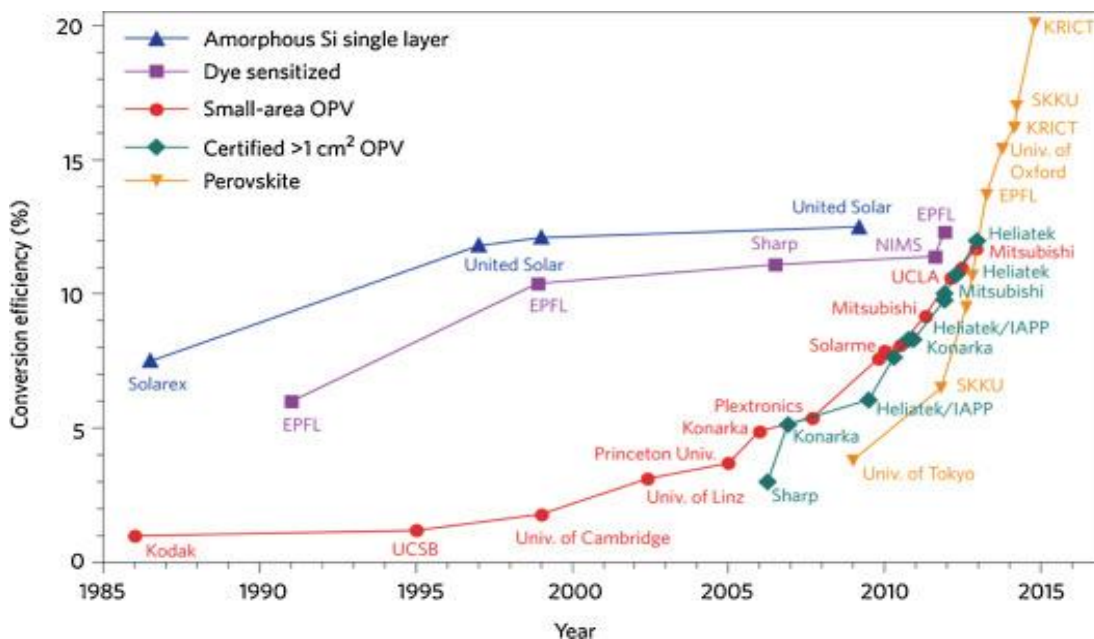


**Figure 1.** NREL Solar Cell Efficiency Chart

But until date, the record-breaking efficiency of the perovskites based devices has risen from 3.8% to 23.3% in recent years [6]. Considering the Goldschmidt Tolerance Factor(GTF),  $\text{CsPbI}_3$  and  $\text{FAPbI}_3$  fall into the category of the established perovskite taking into account the A-site radius of Cs and FA to be 167pm and 253pm respectively [7]. The bandgap of cubic  $\text{CsPbI}_3$  and  $\text{FAPbI}_3$  are 1.73eV and 1.48eV respectively. The interplay of the A-site by the mixed cation ( $\text{FA}^+$  and  $\text{Cs}^+$ ) may result in a wider bandgap and achieving the structural stability of the perovskite making the bandgap nearing to 1.75 eV [8]. The inorganic  $\text{CsPbI}_3$  occurs in two phases namely the yellow non-perovskite phase that exists as orthorhombic crystal structure ( $E_g = 2.78 \text{ eV}$ ) is unstable in the normal environmental conditions and the

stable black perovskite phase which overcomes in the temperature range of 200°C to 300°C as cubic crystal structure. But the organic-inorganic FAPbI<sub>3</sub> resolves by answering to the equilibrium between thermal and structural stability<sup>[9]</sup>.

As a new type of light-harvesting materials is known to possess excellent optoelectronic

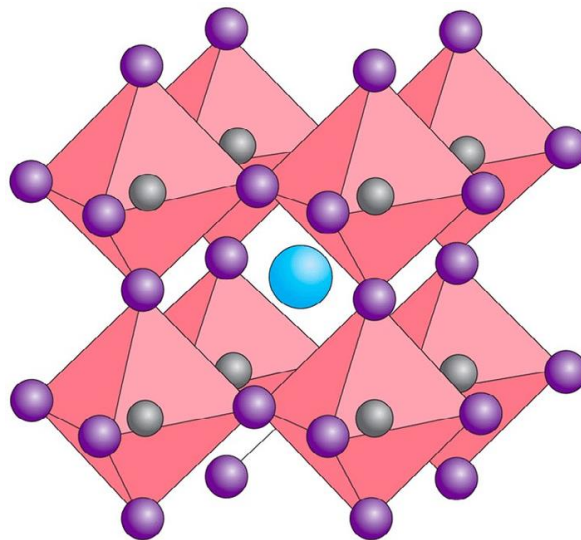


**Figure 2.** Perovskite crystal structure

properties even exceeding those of Methylammonium lead iodide (MAPbI<sub>3</sub>) and Cesium Lead Iodide (CsPbI<sub>3</sub>). The tuning of the A-site by alloying the cesium (Cs<sup>+</sup>) and formidinium (FA<sup>+</sup>) perovskite quantum dots enables the formation of FA<sub>1-x</sub>Cs<sub>x</sub>PbI<sub>3</sub> which show tunable emissions in the IR and near IR range<sup>[10]</sup>.

## 1.2 Solution Processing of Perovskites

Synthesizing the colloidal perovskites quantum dots are focused on mainly two different techniques: (i) ligand assisted re-precipitation and (ii) hot injection method. Overlooking the solution processing aspect, the hot injection method tends to be more advantageous over the

other, as the results would likely to get highly monodispersed quantum dots <sup>[11]</sup>. The hot injection synthesis of the PQDs facilitates distinctive features over those contributed from the conventional film as it enables the grain growth to be decoupled from the assembly of the film. The main problem of implementing the quantum dots in PV application is the presence of long chain organic ligands such as oleates and oleylammonium. These long chain ligands play a crucial role in the formation of the PQDs for improving the charge transporting<sup>[12]</sup>. During the synthesis of PQDs, the cations such as Cs<sup>+</sup>, NH<sub>3</sub><sup>+</sup> and Pb<sub>2</sub><sup>+</sup>, and anions like I<sup>-</sup> and COO<sup>-</sup> assemble themselves to form the PQDs cores. These ligands cooperatively bind with the resulting surface of the QDs which can be influenced by the surface chemistry. Therefore,

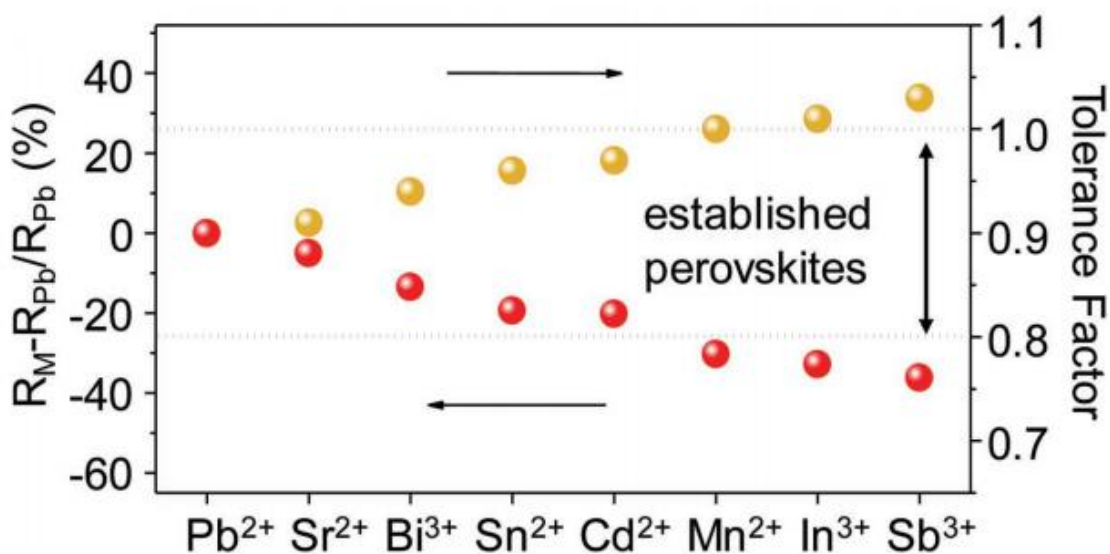


**Figure 3.** Goldschmidt tolerance factor for perovskites cations

removal of these ligands not only improves the stability of the perovskites but also improves the inherent charge transport phenomena. Considering the Goldschmidt tolerance factor the  $\text{CsPbI}_3$  and  $\text{FAPbI}_3$  fall in the category of established perovskite. The interplay of the A-site through the cation exchange mechanism by mixing cations like  $\text{Cs}^+$  and  $\text{FA}^+$  may result in the better structural stability of the PQDs. The presence of the larger cation in PQDs (i.e.,  $\text{FA}_{1-x}\text{Cs}_x\text{PbI}_3$ ) results in fewer surface passivating ligands as compared to the pristine QDs thereby increasing the charge carriers. As mentioned previously, the implementation of surface ligand exchange treatment could improve the inherent charge transport behavior of the PQDs.

The structural stabilization of the PQDs can be improved by the reaction of methyl acetate (MeOAc) during the PQD purification. MeOAc separates the PQDs without full elimination of surface species which is a critical factor for structural stability<sup>[13]</sup>. The assembly of the PQDs as the film involves the presence of surface passivating ligands like oleates and oleylammonium bound to the surface of the PQDs hinder the charge carrier transport. Therefore, to carefully examine the characteristic transport property of the PQDs, the ligands should be eliminated. Ligand exchange for the PQDs can increase the stability and performance of the device. Hence by removing the outbound ligand on the surface, we could naturally study the characteristics charge transfer properties as well as compare these PQDs. After eliminating the surface ligands, we can easily compare the charge carrier's inherent properties of the PQDs<sup>[14]</sup>.

In this work, we present a simple hot injection for the preparation of the CsPbI<sub>3</sub>, FAPbI<sub>3</sub> quantum dots and also have studied the electrical properties of these quantum dots by incorporating in the photodetector. Also, cation exchange is precisely done between these quantum dots to attain Cs<sub>x</sub>FA<sub>1-x</sub>PbI<sub>3</sub>. We have studied the optical properties for the quantum dots synthesized for confirmation of the photoluminescence and absorbance spectra. During the process of synthesis, the crystalline structure of the perovskites is accomplished by the stoichiometric ratios between long-chain organic ligands (oleylammonium: R-NH<sub>3</sub><sup>+</sup> and oleic acid: R-COO<sup>-</sup>). However, the perovskite is terminated by these ligands, binds to the surface of the quantum dots in the process of fabrication of the device. For the optoelectronic devices, there should be a strong pairing between the quantum dots which is accomplished by further purification of the materials as well as the removal of remaining precursors and replacing the ligands with suitable surface species resulting from an increased coupling between the quantum dots. For studying the electronic properties, first, we opted the fabrication of film through simple spin coating. Later, the fabrication of the film was done in various humidity conditions. Ligand exchange is being done carefully, to selectively remove ligands and improve the coupling between the quantum dots which are incorporated on the photodetector. For this, we used the Sodium acetate treatment and FAI treatment in order to decrease the distance of each quantum dot and improve the pairing between them. In the first exchange process, the oleic acid ligand is removed completely and in the post treatment process the ammonium ligand are removed. For this we have evidence from the FT-IR showing the reduction in the (-NH<sub>3</sub><sup>+</sup>) shift. Also from the photoluminescence and absorption spectra we could confirm



the red-shift phenomena while the ligand exchange is done each time. Photocurrent measurements were made with the as-fabricated devices under inert atmospheric conditions. The detectivity and responsivity of the devices were calculated. We also studied the photo-response of the devices <sup>[13]</sup>. We conclude that FAPbI3 shows the highest detectivity and responsivity as well as a high on/off ratio as compared to the other devices.

## 2. EXPERIMENTAL SECTION

**Chemicals:** Cesium carbonate ( $\text{Cs}_2\text{CO}_3$ ; 99.9%), Oleic Acid (OA; technical grade, 90%), Oleylamine (OAm; technical grade, 70%), 1-Octadecene (1-ODE; technical grade, 90%), Hexane (reagent grade,  $\geq 95\%$ ), Octane (anhydrous,  $\geq 99\%$ ), Methyl Acetate (MeOAc, anhydrous, 99.5%), Ethyl Acetate (EtOAc, anhydrous, 99.8%), Formamidinium Acetate (FA-acetate, 99%), Toluene (reagent grade, 99.8%) and Lead Iodide ( $\text{PbI}_2$ ; 99.9985%) were purchased from Sigma-Aldrich.

### 2.1 Synthesis of Cs-Oleate Precursor.

$\text{Cs}_2\text{CO}_3$  (0.407g, 1.25mmol), ODE (20ml) and Oleic acid (1.25ml) were added in a 3-neck round bottom flask and degassed for 30 min at  $60^\circ\text{C}$  and heated to  $150^\circ\text{C}$  in nitrogen until the clear appearance of a solution is observed. Then the Cs oleate was maintained at  $80^\circ\text{C}$  and preheated to  $100^\circ\text{C}$  before use.

### 2.2 Synthesis of FA-Oleate Precursor.

The FA oleate was synthesized by following a previously reported method with slight modifications. Formamidinium Acetate (0.521g, 5mmol) and ODE (16mL) were mixed in a 50mL 3-neck round bottom flask and heated to  $50^\circ\text{C}$  for 30 min under vacuum. Then it is heated to  $120^\circ\text{C}$  in nitrogen until the formation of a clear red colored solution. It was degassed at  $50^\circ\text{C}$  for 30 min and heated to  $100^\circ\text{C}$  for usage.

### 2.3 Synthesis of CsPbI<sub>3</sub>

0.5g PbI<sub>2</sub> and 25mL ODE were heated at 120°C under vacuum for 30 min in a 3-neck round bottom flask. 2.5mL of OA and 2.5mL of OAm was preheated to 120°C and injected into the reaction mixture and degassed for another 30 min until the PbI<sub>2</sub> dissolves and the solution becomes clear. Then it is heated to 165°C under nitrogen. At 165°C, 2mL of the as-synthesized Cs-Oleate was swiftly injected and immediately the reaction mixture was placed in an ice bath. For the purification of the QDs, 70mL of MeOAc was added to the stock and centrifuged at 5000rpm for 10 min. The precipitate was then redispersed in 5 mL of anhydrous hexane and precipitated in 5 mL of MeOAc, and centrifuged at 5000rpm for 10 min. The QDs were then redispersed in 20 mL anhydrous hexane and stored in the refrigerator. Before using the QDs, the solution is taken from the refrigerator and centrifuged at 5000rpm for 10 min. The resulting supernatant is dried and finally, the QDs were redispersed in octane.

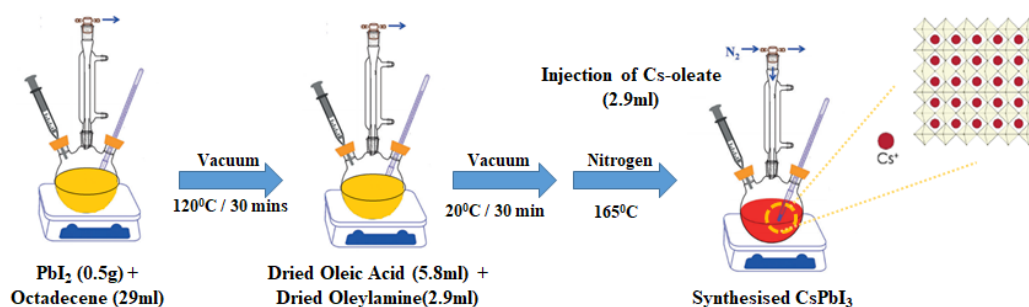


**Figure 4.** Schematic representation of the synthesis of CsPbI<sub>3</sub>

## 2.4 Synthesis of FAPbI<sub>3</sub>

0.344g PbI<sub>2</sub> and 25mL ODE were degassed for 30 min at 120°C in a 3-neck round bottom flask. 4 mL of OA and 2 mL of OAm was preheated to 120°C and injected into the reaction mixture and maintained in vacuum for another 30 min until the PbI<sub>2</sub> dissolves and the solution becomes clear. Then under nitrogen flow, it is cooled to 80°C. At 80°C, 5 mL of FA-Oleate is quickly injected into the PbI<sub>2</sub> solution. After 5 ~ 10sec, the reaction is quenched in an ice bath. To the stock solution, 1mL of toluene and 5 mL of MeOAc were mixed and centrifuged at 5000rpm for 45 min. 7 mL of toluene and 5 mL of MeOAc were added to redisperse and precipitate respectively and centrifuged at 5000rpm for 30 min. Finally, the precipitate is redispersed in 4 mL of anhydrous octane.

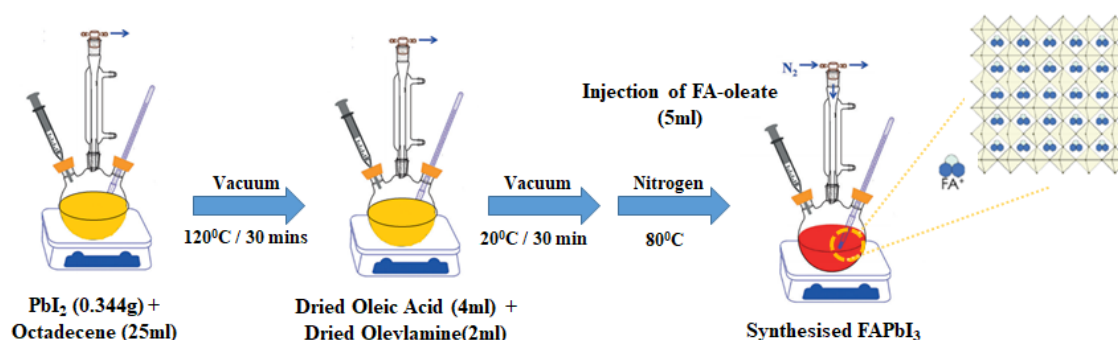


**Figure 5.** Schematic representation of the synthesis of FAPbI<sub>3</sub>

## **2.5 Synthesis of $\text{FA}_{1-x}\text{Cs}_x\text{PbI}_3$**

For the synthesis of  $\text{FA}_{(1-x)}\text{Cs}_{(x)}\text{PbI}_3$ , the optical densities of the colloidal solution of  $\text{CsPbI}_3$  and  $\text{FAPbI}_3$  are matched and mixed in appropriate ratios to obtain the proper stoichiometry.

This was done by adding both the solutions and allowing it to react overnight at  $85^\circ\text{C}$ .

### **3. CHARACTERISATION**

#### **3.1 UV-Vis Spectroscopy**

Absorbance spectroscopy of the PQDs dispersed in hexane were recorded in 1 cm path length quartz cuvettes using Cary 5000 UV-vis-NIR (Agilent technologies) spectrophotometer.

#### **3.2 Photoluminescence spectroscopy**

PL spectra of the PQDs dispersed in hexane were recorded using a Cary Eclipse fluorescence spectrophotometer ( $\lambda_{exc} = 400\text{nm}$ ).

#### **3.3 Time resolved PL spectra**

The TRPL spectra were measured using time correlated single photon counting system (Picoquant, Fluotime 200). The PL emission from the samples was collected by a pair of lenses into the concave holographic gating of 1200 g/mm and detected by photomultiplier tubes (PMT). The temporal resolution and repetition rates are 80 ps and 10MHz respectively. The samples were excited with 375 nm pulses (LDH-P-C-375,  $3\mu\text{W}$ ) at room temperature.

#### **3.4 X-Ray diffraction (XRD)**

XRD patterns were obtained by using Rigaku MiniFlex 600 diffractometer equipped with Cu  $K\alpha$  X-Ray source ( $\lambda = 1.5418 \text{ \AA}$ ). Samples for XRD measurements were prepared by drop casting the purified PQDs on a 1cm \* 1cm glass substrate.

#### **3.5 Transmission Electron Microscopy**

TEM and High-resolution TEM (HRTEM) images were obtained using Hitachi HF-3300 microscope operating at 300 kV. TEM samples were prepared by dropping diluted solution of PQDs onto carbon coated 200 mesh nickel grids.

### **3.6 Fourier-Transform Infra-Red spectroscopy**

FTIR spectra of the PQDs were obtained using Bruker-AVANCE III 400. The PQDs samples were coated directly onto a glass substrate through spin coating and measured in the wave-number between 1250 – 4000  $\text{cm}^{-1}$ .

## 4. Results and discussion

We have successfully synthesized the perovskite quantum dots (PQDs) through hot injection technique by following the procedure reported by Protesescu *et al.* For the preparation of the alloyed compound i.e.  $\text{FA}_{1-x}\text{Cs}_x\text{PbI}_3$ , we have followed the previous studies reported by Hazarika *et al* with a negligible modification. The Figure 6(a-c) shows the high resolution transmission electron microscopy (HR-TEM) images of the perovskites samples prepared from solution phase. We can see that  $\text{FA}_{1-x}\text{Cs}_x\text{PbI}_3$  retains the cubic morphology of the parent  $\text{CsPbI}_3$  and  $\text{FAPbI}_3$  with lattice d-spacing of 3.1nm for  $\text{CsPbI}_3$ , 3.14nm for  $\text{FACsPbI}_3$ , 3.18nm for  $\text{FAPbI}_3$ . The phase confirmation of the perovskites samples is studied through X-ray diffraction (XRD). The cubic phase (pm-3m) is dominant in the spectroscopy which proves the structural stability of the respective PQDs. The photoluminescence and UV-vis spectra of the pristine PQDs are shown in Figure 6(d). The as synthesized colloidal nanocrystals are broadly tunable in the light spectrum especially in the range of 650nm ~ 800nm. The PQDs shows emission at 683nm for  $\text{CsPbI}_3$ , 731nm for  $\text{FA}_{1-x}\text{Cs}_x\text{PbI}_3$  which confirms the exact A-site composition to be in equal and, 777nm for  $\text{FAPbI}_3$ . The change is observed when the materials are incorporated into the film showing a significant red shift. Compared to the X-site (anion exchange mechanism), the A-site (cation exchange mechanism) requires well controlled temperatures alloying for the formation of  $\text{FA}_{1-x}\text{Cs}_x\text{PbI}_3$ .



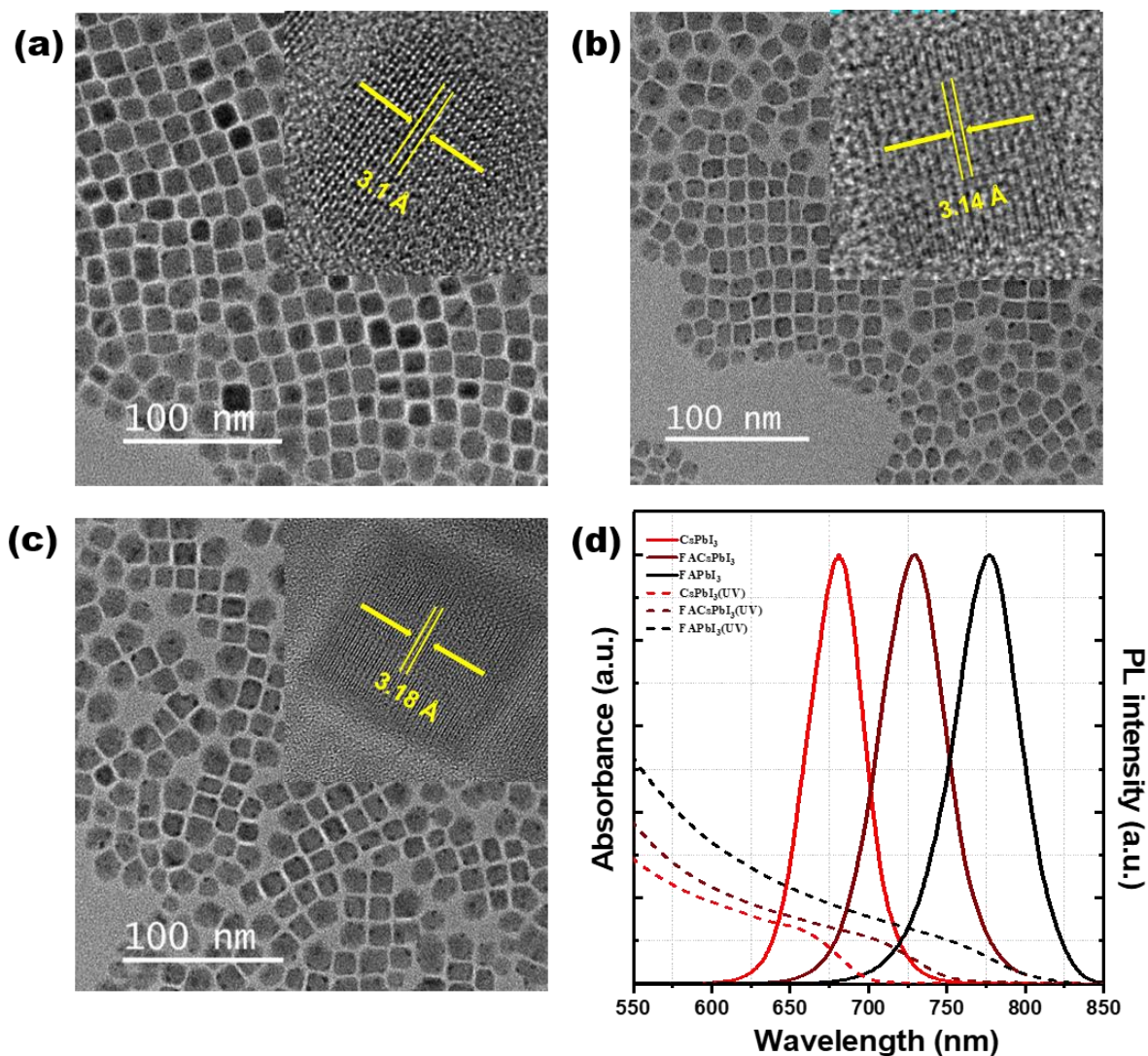


**Figure 6.** Transmission electron microscopy images of (a) CsPbI<sub>3</sub> (b) Cs<sub>1-x</sub>FA<sub>x</sub>PbI<sub>3</sub> (c)FAPbI<sub>3</sub> nanocrystals and (d) Photoluminescence of the solution samples. Inset figure shows the HRTEM of single nanocrystal.

We execute the process at different temperatures based on previous studies, but 80°C processing of the parent PQDs is positive for our work. The time dependant photoluminescence observation shown in supporting information shows the formation of Cs<sub>(1-x)</sub>FA<sub>(x)</sub>PbI<sub>3</sub> by the alloying of PQDs. From this figure we can see that the initial peaks of the parent CsPbI<sub>3</sub> and FAPbI<sub>3</sub> gradually merge to form FAcPbI<sub>3</sub> overtime. The presence of smaller cation such as Cs<sup>+</sup> when combined with larger cation like FA<sup>+</sup> tends to lower the effective radius of the alloyed

perovskite. This nearly equals the tolerance factor of the cubic lattice structure which corresponds to the black perovskite phase. Thereby, the black perovskite phase is almost preferred as the alloyed compound would likely to suppress the yellow hexagonal phase which is not entropically stable. The thermal and structural instability mainly occur in the native perovskite structure, hence the need for alloying the parent PQDs i.e. CsPbI<sub>3</sub> and FAPbI<sub>3</sub> is essential to succeed the above mentioned factors. We fabricated the perovskite QDs dispersed in octane on the substrate through spin coating method as previously mentioned work. For the inherent ligand removal and incorporation of FA<sup>+</sup> on the surface of the QDs, we first treated the film with a saturated solution of sodium acetate solution in methyl acetate after fabricating each layer. Finally, as a post-treatment process we finally immersed with a saturated solution of AX salt (Formamindium Iodide salt) to complete the ligand exchange with FA<sup>+</sup>. Figure 6 represents the schematics of ligand removal of each QD in a stepwise manner for the assembly of film. For the CsPbI<sub>3</sub>, in the first step of ligand exchange, the removal of oleic acid ligand tends to be the maximum as the A-site does not contain any of the FA<sup>+</sup> in it. But looking forward on the other QDs, there tends to be little different case as the A-site of the QDs contain FA<sup>+</sup>.

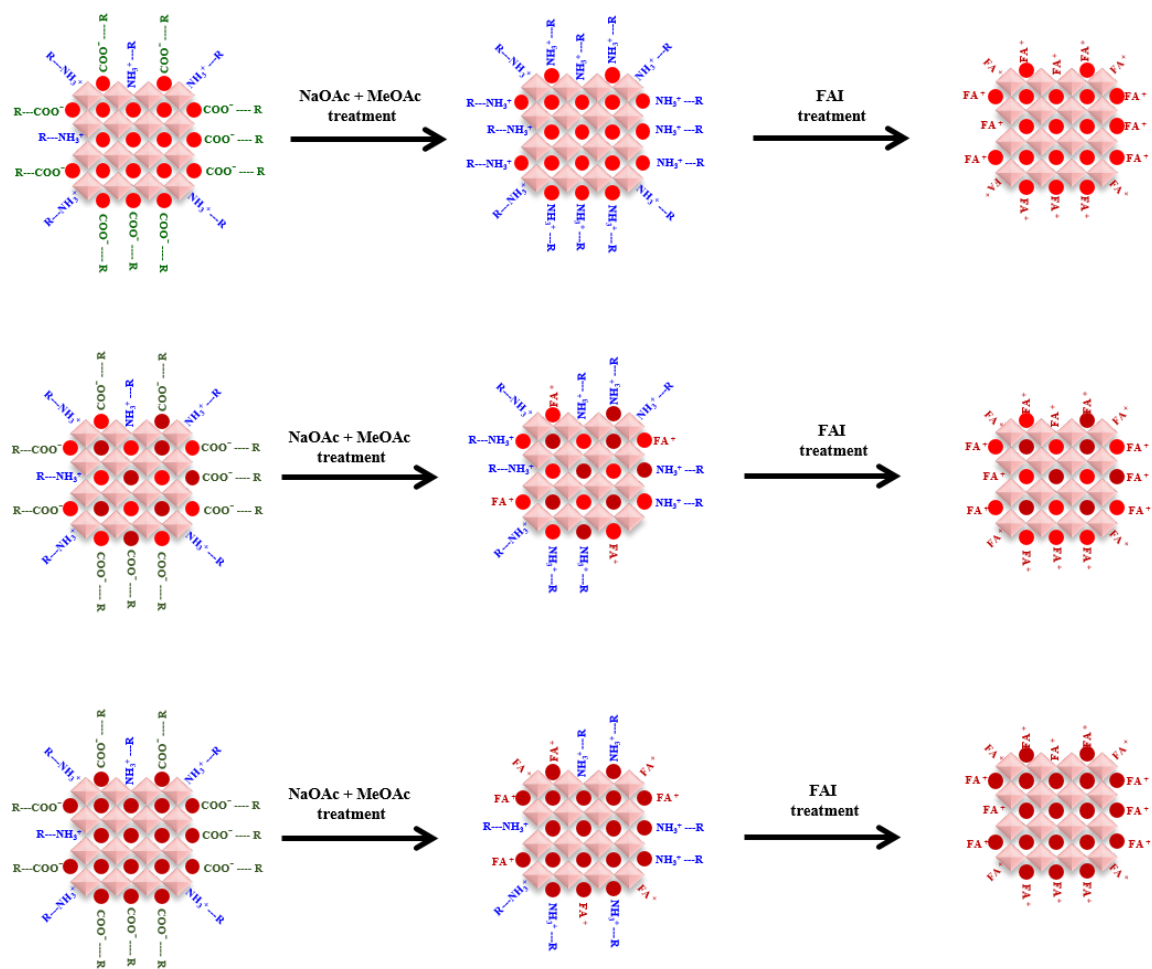


**Figure 7.** Schematic representation of removal of long chain oleic acid and oleylammonium ligand and incorporation of  $FA^+$  cations.

In case of  $\text{FA}_{(1-x)}\text{Cs}_x\text{PbI}_3$ , after the first ligand exchange process, we could sense some  $\text{FA}^+$  has already been incorporated on the surface of the QD. In the last case of the  $\text{FAPbI}_3$ , the oleic acid has been completely removed and the amount of  $\text{FA}^+$  incorporation is the maximum.

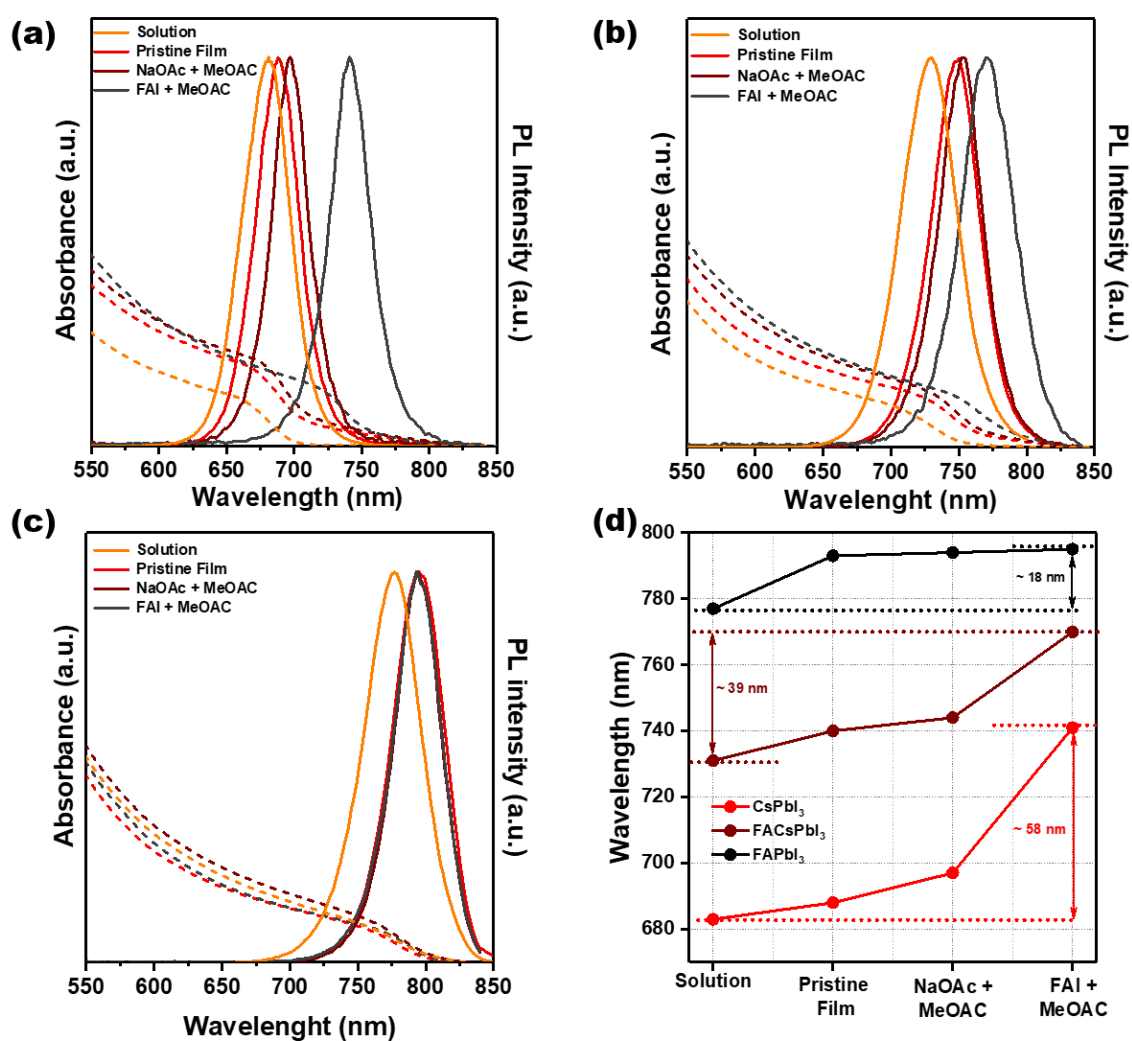


**Figure 8.** Shifting of PL peaks in the process of ligand exchange (a)  $\text{CsPbI}_3$  (b)  $\text{FA}_{1-x}\text{Cs}_x\text{PbI}_3$  (c)  $\text{FAPbI}_3$  nanocrystals and (d) Summarized chart representing the peak position shift.

This reaction is known to be as the Ester hydrolysis that particularly occurs in the controlled humidity environment in which the moisture in the atmosphere helps to generate acetic acid and methanol from methyl acetate. In the process of post treatment with FAI the removal of the oleylamonium ligand occurs as the  $\text{FA}^+$  completely gets bound on the surface of the QDs. This is more significant in the  $\text{CsPbI}_3$ , as it contains only the ligands and no other  $\text{FA}^+$  cations incorporated on the surface. The purpose of treating with FAI and ethyl acetate is to specifically target the oleylamonium ligands and replace with  $\text{FA}^+$  cations. Figure 8 shows the evidence from the photoluminescence spectra of the QDs after each process. There seems to be a shift of the spectra when the QDs are assembled as film.

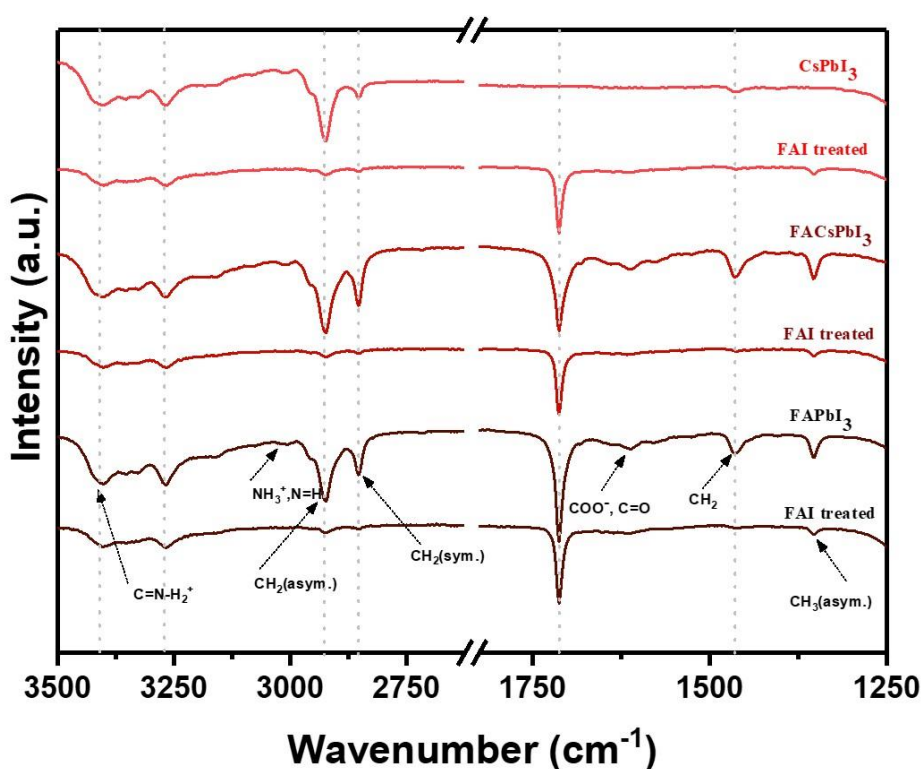


**Figure 9.** FTIR spectroscopy of pristine and ligand exchanged samples of the PQD film.

In case of the spectra of solution samples, the emission occurs from directly from the QDs. When dispersing the samples in non-polar solvents like hexane, the particles free themselves from the ligands and the distance between each QDs are very much large. But assembling the QDs as film, the distance between the QDs becomes minimum and ligands confines themselves on the surface. Therefore, we could observe a slight red shift in the spectra. Yet again, the spectral shift is observed when comparing the pristine film sample and first ligand exchange treatment process.

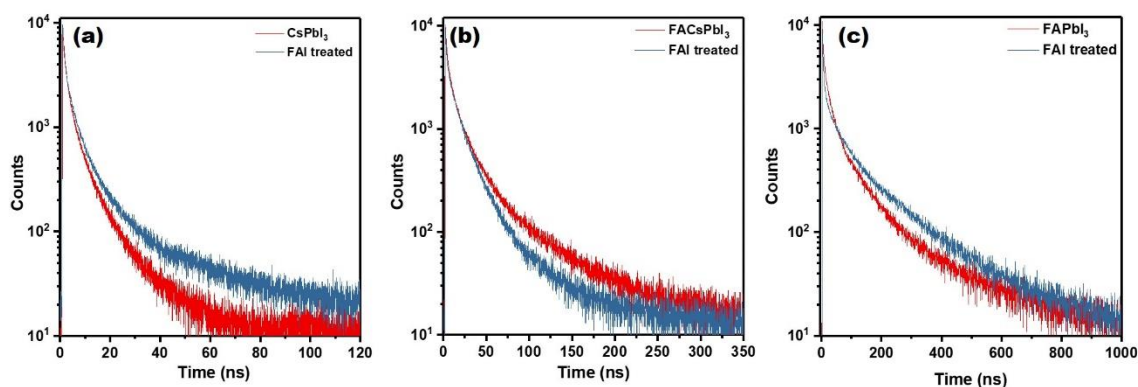


**Figure 10.** Time resolved spectroscopy of pristine and ligand exchanged samples of the PQD film.

This is owed to point that oleic acid ligand is completely removed from the surface of the QDs. In the final post treatment process, we could observe a huge red shift of the spectra (in case of CsPbI<sub>3</sub> & FA<sub>(1-x)</sub>Cs<sub>(x)</sub>PbI<sub>3</sub>) and a very marginal shift (in case of FAPbI<sub>3</sub>) due the removal of oleylamonium ligand and incorporation of FA<sup>+</sup> on the surface. Figure 8(a-c) shows the shift of photoluminescence spectra of the CsPbI<sub>3</sub>, FA<sub>(1-x)</sub>Cs<sub>(x)</sub>PbI<sub>3</sub> & FAPbI<sub>3</sub> respectively. We have compared each spectra obtained after each process. Figure 8d represent the summarised photoluminescence shift of each QDs. We observed that the change of PL spectra of FAPbI<sub>3</sub> tends to be the small as compared to the others as the surface of QDs has been already incorporated

with maximum number of  $\text{FA}^+$ . Also the  $\text{CsPbI}_3$ , has the maximum shift of PL spectra as more number of oleylamonium ligand is replaced with  $\text{FA}^+$ .

To confirm the ligand exchange process, we further investigate through Fourier transform infrared spectroscopy (FTIR) spectra for the PQDs as shown in Figure 9. We measured the spectra of the PQDs for pristine sample as well as for the ligand exchanged samples. For the pristine samples, we could observe the  $-\text{CH}_2$  symmetric and asymmetric stretching in the range of  $2840 - 2950 \text{ cm}^{-1}$  and  $-\text{CH}_2$  bending at  $1466 \text{ cm}^{-1}$ . The carboxylic group bending can be observed in the range of  $1640 \text{ cm}^{-1}$  which originates from the oleic acid and oleylamonium. When the ligand exchange process is done we could witness that the bending vibration is completely decreased confirming the removal of oleic acid and oleylamonium. The excess peaks for the  $\text{CsPbI}_3$  confirms the successful incorporation of  $\text{FA}^+$  on the QD surface.

Further time resolved photoluminescence spectroscopy (TRPL) was conducted to obtain the confirmation of surface ligand exchange removal. TRPL is mainly executed for the examination of exciton lifetime according to the surface passivation which is done with short chain ligand ( $\text{FA}^+$ ). Figure 10(a-c) shows the TRPL analysis for the perovskite QDs before and after ligand exchange process. From the figure, we could say that the exciton lifetime is increased as the surface passivating ligand decreased after the ligand exchange is carried out. This tells the fact that when the exciton lifetime is increased the non-radiative recombination is dramatically reduced. The TRPL decay curve deviates from single to multi exponential as the surface passivating ligand decreases. Therefore, we could confirm that the long chain oleic acid and oleylamonium were passivated with the  $\text{FA}^+$  successfully.

# **PART 2**

## **Application of PQDs in Photodetector**



## 1. Introduction

Photodetector is a device that converts light signals into electrical signals and acts like a human eye. The important parameters include spectral response range, sensitivity, response time, EQE and stability. At present the most widely used photodetectors in business are based on silicon materials. However, the high cost may provide limitations on their applications. Recently, solution-processable perovskites with a lower trap density, high quantum efficiency, small exciton binding energy, long carrier diffusion length and long life of carrier is becoming an ideal material for highperformance photodetectors. According to the configuration of devices, perovskite photodetectors can be divided into three types: photoconductors, photodiodes and phototransistors.

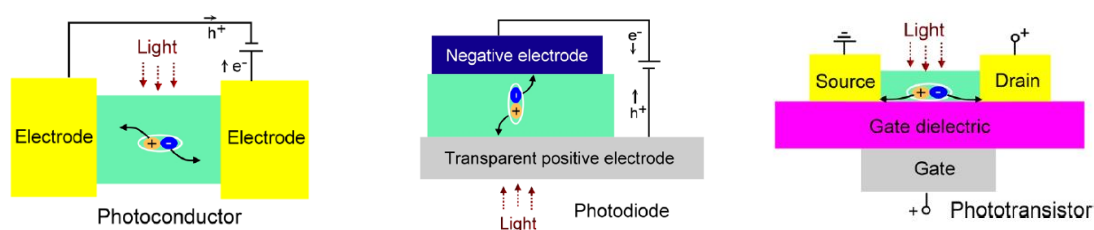


**Figure 11.** Representation of types of photodetectors

Perovskites-based photoconductors have an obvious merit of relatively facile fabrication process, using metal–semiconductor–metal structures. However, the large dark current usually forms ohmic contact, and the large applied voltage limited the detectivity. In 2014, however, solution-processed MAPbX<sub>3</sub> was first used as a photoconductor for a broadband wavelength from 310 to 780 nm. Although the rise time and decay time were about 0.2 s<sup>-1</sup>, the EQE reached 1.19 × 103 % at 365 nm<sup>[16]</sup>. In fact, this structure showed the original properties of perovskites

and was easily for encapsulation to achieve a stable device, such as the use of a water-resistant fluorinated polymer to increase the device stability<sup>[17]</sup>.

Furthermore, a photodiode with p-n, p-i-n, or Schottky junction provides a fast response speed and high detectivity. This is because the built-in electrical field at the junction interface can promote the extraction of photoexcited carriers at low driving voltages. Therefore, in 2016, a diode-type photodetector based on perovskites as the active layer showed ultrafast response time of  $\approx 1$  ns with operation at zero bias owing to the high mobility of perovskite layer and low trap density<sup>[18]</sup>. However, the use of ITO may limit its application for UV-region detection due to the strong absorption of ITO below the light wavelength of 350 nm.

A phototransistor with a gate electrode is a reasonable device design to increase the photoresponsivity without sacrificing the response speed. For example, ambipolar solution-processed perovskites phototransistors showed a dark current less than 0.5 nA and a high photocurrent of 0.1 mA under white-light illumination. After applying a gate voltage, the photogenerated carriers accumulate in the channel, resulting in a higher mobility than other photodetector structures. In addition, the carrier lifetime will be increased owing to the reduced recombination of the photoexcited electron-hole pairs in the perovskites channel,<sup>[19]</sup> and the photoresponsivity can reach  $320 \text{ AW}^{-1}$ , which is higher than commonly used silicon photodetectors ( $\sim 300 \text{ AW}^{-1}$ ). Photodetector plays an important role in signal processing, communication, and biological imaging.

FET is an archetype of electronic devices. Although the high-mobility silicon crystal semiconductors have been widely used in modern electronics, they are expensive, heavy, and often require high-temperature preparation .

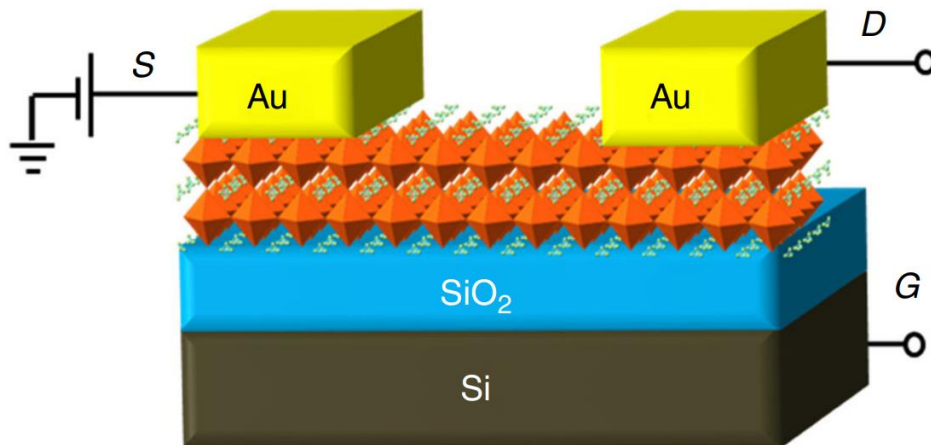


**Figure 12.** Perovskite-based FET device

Organic semiconductors, on the other hand, can be processed by low-cost solution methods, but weak van der Waals interactions between molecules limit the mobility of carriers. Molecular-level composite of organic and perovskites partners may enjoy the advantages of solution processing and high mobility. The inorganic components form frameworks that combine via covalent or ionic bonds to increase carrier mobility. Organic components promote the overall self-assembly of perovskite materials and create an opportunity for solution processing. By designing suitable organic components, the energy levels and dimensions of the perovskites could be changed and improved the performance of FETs.

## 2. Device Fabrication

PQD films were fabricated using previously reported methods (4). Saturated Sodium Acetate (NaOAc) in MeOAc solution and AX salt (where AX = FAI) in EtOAc solution were prepared by sonicating 20 mg of NaOAc (or AX salt) and 20 ml of MeOAc (or EtOAc) for 10 min. Because all the salts were only slightly soluble in their corresponding solvent, excess salt was removed via centrifugation at 3500 rpm for 5 min. Each layer of PQDs was spincoated from a concentrated QD solution in octane (~75 mg/ml) at spin speeds of 6000 rpm for 20s. The film was then briefly dipped (~1 s) into the NaOAc in MeOAc solution, rinsed in a solution of neat MeOAc, and then immediately dried in a stream of dry air.

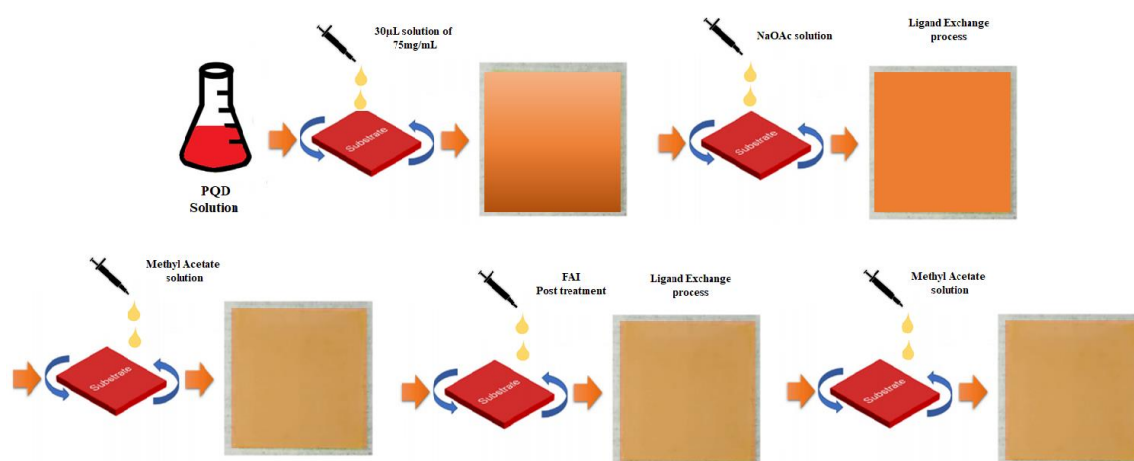


**Figure 13.** Ligand Exchange process of PQDs

This process of spin-coating PQDs and dipping in NaOAc in MeOAc solution was repeated two to three times to achieve a total film thickness of 100 to 300 nm. Once the desired film thickness was achieved, the films were posttreated by soaking the film in the AX salt in EtOAc solution for 10 s before rinsing in MeOAc and then immediately drying under a stream of dry

air. All film fabrications were carried out under dry ambient conditions (relative humidity, ~16 to 20%).

### 3.Results and Discussion

For better understanding of the inherent charge transfer properties of the PQDs on their photoresponse performance, transistor-type photodetectors were fabricated with  $\text{CsPbI}_3$ ,  $\text{Cs}_{1-x}\text{FA}_x\text{PbI}_3$ ,  $\text{FAPbI}_3$ . For the fabrication of the device, we first deposit 100nm thick  $\text{SiO}_2$  on a silicon substrate and later gold electrodes are patterned on using lithography technique.

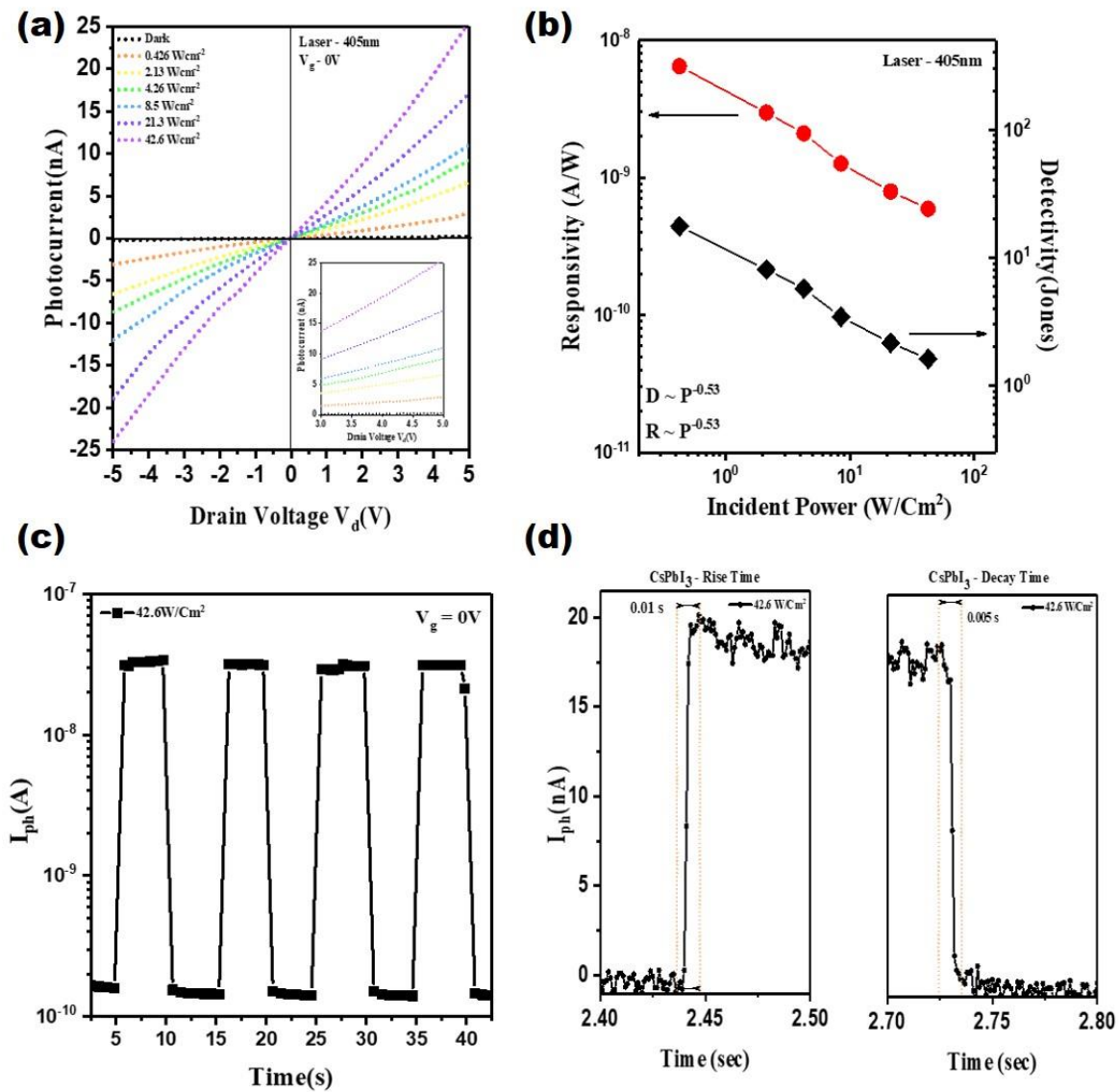


**Figure 14.** (a) I-V characteristics of  $\text{CsPbI}_3$  as a function of incident light intensity. (b) Dependence of responsivity and detectivity on incident power of  $\text{CsPbI}_3$  photodetector measured at  $V_d = 5\text{V}$  and  $V_g = 0\text{V}$ . (c) Photocurrent-Time ( $I_{ph}$ -t) response measured in dark and under illumination using a laser

source at 405nm. **(d)** Time resolved analysis of rise and decay time @42.6W/cm<sup>2</sup>.

A uniform film of the perovskites was assembled on the device to check the performance. The width of the channel is 3 $\mu$ m. Figure 14(a), 15(a) & 16(a) shows the I-V curve of the colloidal nanocrystals in the dark and under laser light of 405nm with incident power ranging from 0.426 to 42.6W/Cm<sup>2</sup>. We can see that the behaviour of the I-V is linear which tells that device has a good ohmic contact between the electrodes and perovskite QDs. In the applied dark state, the photocurrent obtained is nearly in the range of Pico ampere. Under illumination,

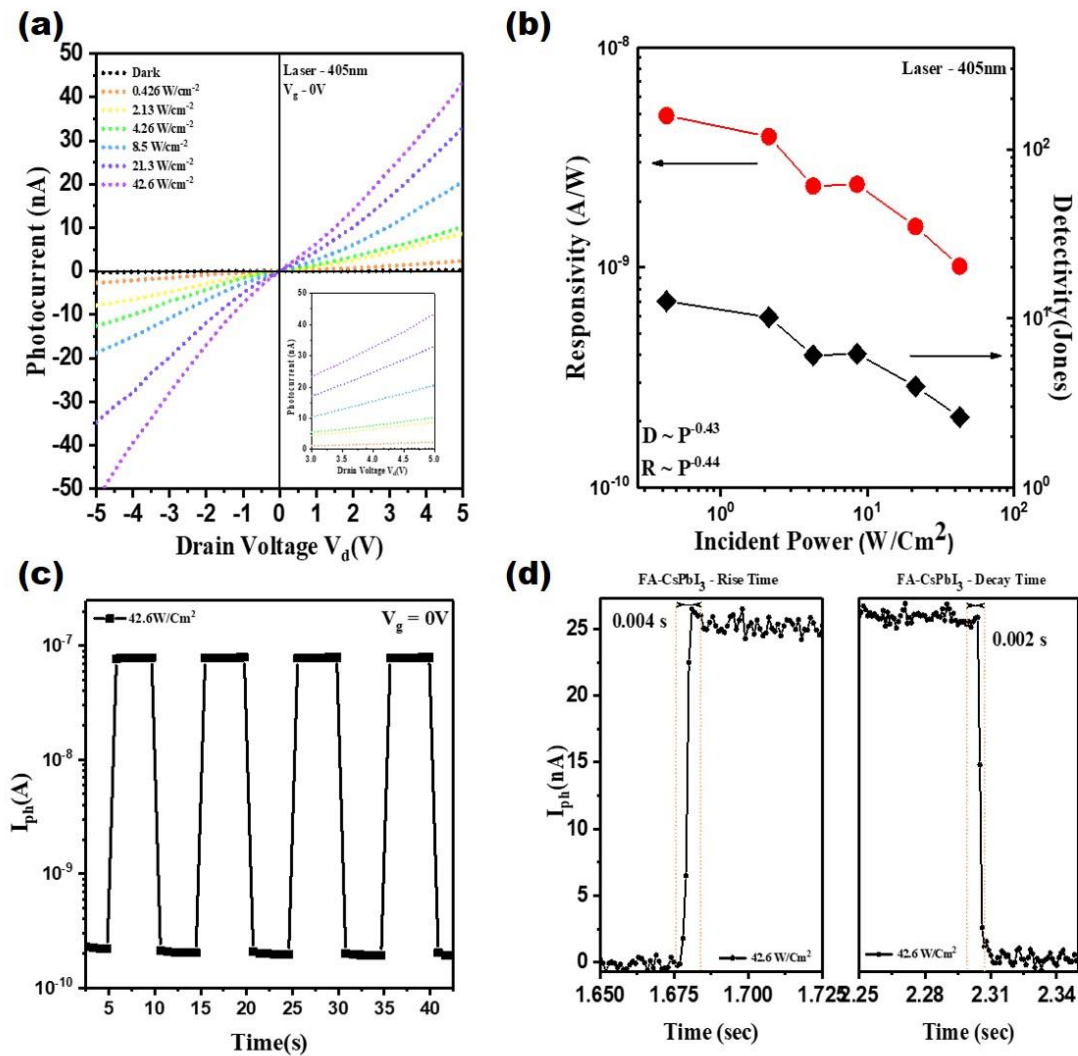


**Figure 15. (a)** I-V characteristics of  $\text{FA}_{1-x}\text{Cs}_x\text{PbI}_3$  as a function of incident light intensity. **(b)** Dependence of responsivity and detectivity on incident power of  $\text{FA}_{(1-x)}\text{Cs}_{(x)}\text{PbI}_3$  photodetector measured at  $V_{\text{ds}} = 5\text{V}$  and  $V_{\text{g}} = 0\text{V}$ . **(c)** Photocurrent-Time ( $I_{\text{ph}}-t$ ) response measured in dark and under illumination using a laser source at 405nm. **(d)** Time resolved analysis of rise and decay time @42.6W/cm<sup>2</sup>.

photon absorption occurs and consequently large amount of electron-hole pairs are generated over the applied electric field. Compared to the pristine film of the perovskite samples, the FAI treated film show much higher photocurrent. Among the 3 perovskite QDs device,  $\text{FAPbI}_3$  shows the highest photocurrent gain under the maximum incident power. This fashion is observed across the devices as the number of surface ligand removal in initial stages makes strong coupling in the QDs and in the post treatment of the devices with metal halide salt, the strong interaction transforms into bulk perovskite film. From the Figure 13(b), 14(b) & 15(b), the



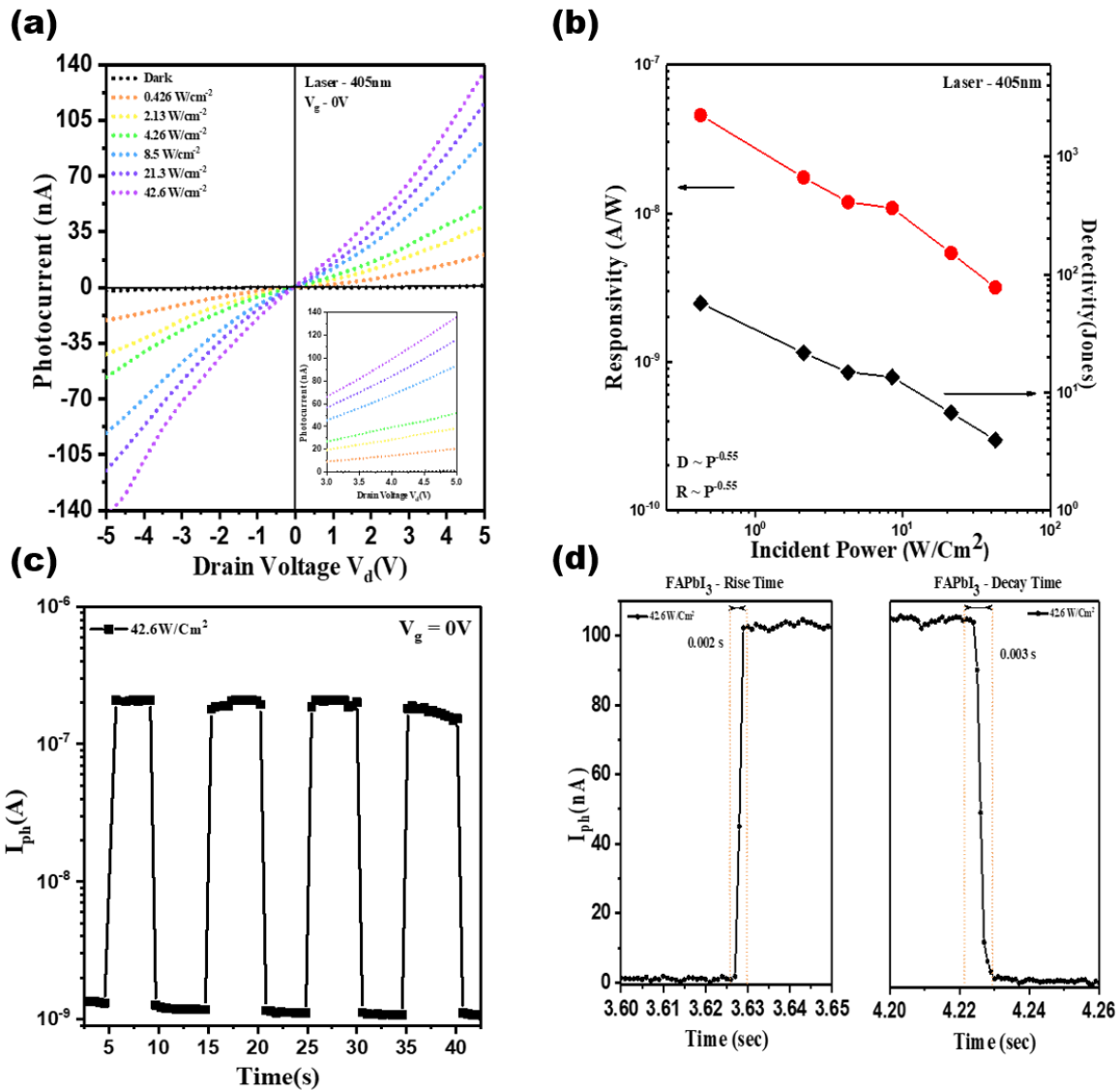


**Figure 16.** (a) I-V characteristics of FAPbI<sub>3</sub> as a function of incident light intensity. (b) Dependence of responsivity and detectivity on incident power of FAPbI<sub>3</sub> photodetector measured at  $V_{ds} = 5V$  and  $V_g = 0V$ . (c) Photocurrent-Time ( $I_{ph}$ -t) response measured in dark and under illumination using a laser source at 405nm. (d) Time resolved analysis of rise and decay time @42.6W/cm<sup>2</sup>.

detectivity and responsivity of the device can be easily extracted. The responsivity is defined as the ratio of photocurrent ( $I_{ph} - I_{dark}$ ) divided by the incident power of the light. Both of the parameters exhibit a sublinear dependency of the optical power, which can be fitted using the power law,  $I_{ph} \sim P^\alpha$ . The process of electron-hole pair generation, recombination and trapping

within the material gives the non-unity exponent fit ( $0.5 < \alpha < 1$ ). The equivalent  $D^*$  (Jones) was found out using the relation,  $D^* = R/(2eI_{\text{dark}}/A)^{0.5}$ , where  $R$  is the responsivity of the device,  $e$  is the charge of the electron ( $1.6 \times 10^{-19}$ ) C,  $I_{\text{dark}}$  is the dark current of the device and  $A$  is the area of the device. Photoresponse i.e., the rise and decay time of the device when light is switched ON/OFF is one of the main figure of merits. Figure 14(c), 15(c) & 16(c) shows the photoresponse characteristics of each device respectively. Laser light of 405nm was used to measure the photoresponse of each device. We have also made the time resolved photoresponse analysis of each device which shows in detail the rise and decay time which is represented in the Figure 14(d), 15(d) & 16(d).

#### **4. Conclusions**

We optimised the synthesis parameters for PQDs and cation exchange of  $\text{Cs}_{1-x}\text{FA}_x\text{PbI}_3$ . By the ligand exchange method, we could replace the long chain ligands with short chain ligands (FA cations). By the characterisation techniques, we confirmed the replacement of long chain ligands. We implemented the PQDs on the photodetector for investigating the inherent charge transport through photoresponse. Among the 3 PQDs used we say that  $\text{FAPbI}_3$  is the best in case of photocurrent gain and photoresponse. Also the detectivity and responsivity of the  $\text{FAPbI}_3$  was the highest compared to other PQDs.

## References

- [1] He Huang, Maryna I. Bodnarchuk, Stephen V. Kershaw, Maksym V. Kovalenko, and Andrey L. Rogach. Lead Halide Perovskite Nanocrystals in the Research Spotlight: Stability and Defect Tolerance. *ACS Energy Letters* **2017** 2 (9), 2071-2083.
- [2] He Huang, Lakshminarayana Polavarapu, Jasmina A. Sichert, Andrei S. Susa, Alexander S. Urban and Andrey L. Rogach. Colloidal lead halide perovskite nanocrystals: synthesis, optical properties and applications. *NPG Asia Materials* (**2016**) 8, e328.
- [3] Loredana Protesescu, Sergii Yakunin, Sudhir Kumar, Janine Bar, Federica Bertolotti, Norberto Masciocchi, Antonietta Guagliardi, Matthias Grotevent, Ivan Shorubalko, Maryna I. Bodnarchuk, Chih-Jen Shih, and Maksym V. Kovalenko. Dismantling the “Red Wall” of Colloidal Perovskites: Highly Luminescent Formamidinium and Formamidinium–Cesium Lead Iodide Nanocrystals. *ACS Nano* **2017**, 11, 3119–3134.
- [4] Maksym V. Kovalenko, Loredana Protesescu, Maryna I. Bodnarchuk. Properties and potential optoelectronic applications of lead halide perovskite nanocrystals. *Science* 358, 745–750 (**2017**).
- [5] <https://doi.org/10.1038/s41563-018-0018-4>.
- [6] [www.nrel.gov/pv/assets/images/efficiency-chart.png](http://www.nrel.gov/pv/assets/images/efficiency-chart.png).
- [7] Michael Saliba, Taisuke Matsui, Konrad Domanski, Ji-Youn Seo, Amita Ummadisingu, Shaik M. Zakeeruddin, Juan-Pablo Correa-Baena, Wolfgang R. Tress, Antonio Abate, Anders Hagfeldt, Michael Grätzel. Incorporation of rubidium cations into perovskite solar cells improves photovoltaic performance. *Science* 354, 206-209 (**2016**).
- [8] David P. McMeekin, Golnaz Sadoughi, Waqas Rehman, Giles E. Eperon, Michael Saliba, Maximilian T. Hörantner, Amir Haghighirad, Nobuya Sakai, Lars Korte, Bernd Rech, Michael B. Johnston, Laura M. Herz, Henry J. Snaith. A mixed-cation lead mixed-halide perovskite absorber for tandem solar cells. *Science* 351, 151-155 (**2015**).
- [9] Maksym V. Kovalenko, Loredana Protesescu, Maryna I. Bodnarchuk. Properties and potential optoelectronic applications of lead halide perovskite nanocrystals. *Science* 358, 745–750 (**2017**).

[10] Yupeng Zhang, Jingying Liu, Ziyu Wang, Yunzhou Xue, Qingdong Ou, Lakshminarayana Polavarapu, Jialu Zheng, Xiang Qiao and Qiaoliang Bao. Synthesis, Properties, and optical applications of low dimensional perovskites. *Chem. Commun.*, **2016**, 52, 13637.

[11] Giles E. Eperon, Victor M. Burlakov, Pablo Docampo, Alain Goriely, and Henry J. Snaith. Morphological Control for High Performance, Solution-Processed Planar Heterojunction Perovskite Solar Cells. *Adv. Funct. Mater.* **2014**, 24, 151–157.

[12] Lance M. Wheeler, Erin M. Sanehira, Ashley R. Marshall, Philip Schulz, Mokshin Suri, Nicholas C. Anderson, Jeffrey A. Christians, Dennis Nordlund, Dimosthenis Sokaras, Thomas Kroll, Steven P. Harvey, Joseph J. Berry, Lih Y. Lin, and Joseph M. Luther. Targeted Ligand-Exchange Chemistry on Cesium Lead Halide Perovskite Quantum Dots for High-Efficiency Photovoltaics. *J. Am. Chem. Soc.* (**2018**) 140, 33, 10504-10513.

[13] Dmitri V. Talapin, Jong-Soo Lee, Maksym V. Kovalenko, and Elena V. Shevchenko. Prospects of Colloidal Nanocrystals for Electronic and Optoelectronic Applications. *Chem. Rev.* (**2010**), 110, 389–458.

[14] ABHISHEK SWARNKAR, ASHLEY R. MARSHALL, ERIN M. SANEHIRA, BORIS D. CHERNOMORDIK, DAVID T. MOORE, JEFFREY A. CHRISTIANS, TAMOGHNA CHAKRABARTI, JOSEPH M. LUTHER. Quantum dot-induced phase stabilization of  $\alpha$ -CsPbI<sub>3</sub> perovskite for high-efficiency photovoltaics. *SCIENCE* 07 OCT **2016** : 92-95.

[15] ERIN M. SANEHIRA, ASHLEY R. MARSHALL, JEFFREY A. CHRISTIANS, STEVEN P. HARVEY, PETER N. CIESIELSKI, LANCE M. WHEELER, PHILIP SCHULZ, LIH Y. LIN, MATTHEW C. BEARD, JOSEPH M. LUTHER. Enhanced mobility CsPbI<sub>3</sub> quantum dot arrays for record-efficiency, high-voltage photovoltaic cells. *SCIENCE ADVANCES* 27 OCT **2017** : EAAO4204.

[16] Lance M. Wheeler, Erin M. Sanehira, Ashley R. Marshall, Philip Schulz, Mokshin Suri, Nicholas C. Anderson, Jeffrey A. Christians, Dennis Nordlund, Dimosthenis Sokaras, Thomas Kroll, Steven P. Harvey, Joseph J. Berry, Lih Y. Lin, and Joseph M. Luther. Targeted Ligand-Exchange Chemistry on Cesium Lead Halide Perovskite Quantum Dots for High-Efficiency Photovoltaics. *Journal of the American Chemical Society* **2018** 140 (33), 10504-10513.

- [17] Guo, Y.; Liu, C.; Tanaka, H.; Nakamura, E. Air-Stable and Solution-Processable Perovskite Photodetectors for Solar-Blind UV and Visible Light. *J. Phys. Chem. Lett.* **2015**, *6*, 535–539.
- [18] Shen, L.; Fang, Y.; Wei, H.; Yuan, Y.; Huang, J. A Highly Sensitive Narrowband Nanocomposites Photodetector with Gain. *Adv. Mater.* **2016**, *28*, 2043–2048.
- [20] Dmitri V. Talapin, Jong-Soo Lee, Maksym V. Kovalenko, and Elena V. Shevchenko. Prospects of Colloidal Nanocrystals for Electronic and Optoelectronic Applications. *Chem. Rev.* (**2010**), *110*, 389–458.
- [19] Li, F.; Ma, C.; Wang, H.; Hu, W.; Yu, W.; Sheikh, A.; Wu, T. Ambipolar Solution-Processed Hybrid Perovskite Phototransistors. *Nat. Commun.* **2015**, *6*, 8238.
- [20] Wei, W.; Zhang, Y.; Xu, Q.; Wei, H.; Fang, Y.; Wang, Q.; Deng, Y.; Li, T.; Gruverman, A.; Cao, L.; Huang, J. Monolithic Integration of Hybrid Perovskite Single Crystals with Heterogenous Substrate for Highly Sensitive X-Ray Imaging. *Nat. Photonics* **2017**, *11*, 315–321.

## 요 약 문

광 검출기 응용을 위한 Formamidinium 양이온으로 기능화된 밴드갭  
가변 콜로이드 페로브스카이트 나노 결정

할로겐화 페로브스카이트의 콜로이드 양자점 (PQD)은 태양전지, 레이저 및 발광다이오드 (LED)와 같은 다양한 광전자 분야에서 크기 및 구성 의존 광학 밴드갭 ( $E_g$ ), 흡광 계수, defect tolerance 밴드 구조 및 좁은 밴드 방출과 같은 많은 장점으로 인해 관심을 받고 있습니다. PQD 박막을 제조할 때, 사전에 결정화된 PQD 를 사용하고, 이는 기존 페로브스카이트 박막 제조에 필요한 열 처리가 필요하지 않기 때문에,  $CsPbI_3$ ,  $FAPbI_3$  및  $Cs_{1-x}FA_xPbI_3$  와 같은 PQD 는 상온 및 용액공정 박막 태양전지에서 광-흡수제로 이용되어 왔습니다. 또한, 전하 수송 특성을 분석하기 위해, PQD 는 광 검출기에 사용될 수 있습니다. 낮은 트랩 밀도, 긴 캐리어 수명 및 확산 길이로 인해 PQD 는 광 검출기의 성능을 향상시키는데 이상적인 재료입니다. 또한, PQD 는 입사광을 흡수하고 전자-정공쌍을 생성하는 광 검출기 내의 반도체 물질로 사용됩니다. 광전류는 외부 혹은 build-in 전기장의 적용으로 전하 운반체를 추출한 결과로 생성됩니다. 특히, 물질의 광-투과성이 응답 속도 손실 없이 증가하기 때문에 트랜지스터형 광 검출기가 사용될 수 있습니다. 소자 구동중, 전하 캐리어의 축적을 통해 높은 이동도가 얻어집니다. 또한, 광생성 전자-정공쌍의 감소된 재결합 속도로 인해, 캐리어 수명 시간이 증가됩니다.

본 연구는 음이온성 올레이트와 양이온성 올레일암모늄을 선택적으로 제거하여 PQDs 박막의 고유 전하 수송을 향상시키는 전략을 소개합니다. 먼저, PQD의 광학적 특성을 연구하기 위해, CsPbI<sub>3</sub> 및 FAPbI<sub>3</sub>는 열 주입 방법을 통해 합성되었습니다. CsPbI<sub>3</sub>과 FAPbI<sub>3</sub> 사이의 A-사이트 상호작용은 조절된 양이온 교환 반응을 통해 Cs<sub>1-x</sub>FA<sub>x</sub>PbI<sub>3</sub>의 형성을 유도합니다. 또한, 합성 후 각각의 PQD에 결합된 리간드의 양이 다르기 때문에, 표면에 흡착된 긴 체인 리간드를 짧은 체인 리간드로 제거 및 대체하는 것은 양자점 사이의 커플 링을 향상시킵니다. 또한, 고유 전하 수송 메커니즘을 연구하기 위해, 트랜지스터 타입 광 검출기에 PQD를 적용하는 것은 중요한 관찰로 이어질 수 있습니다.

## **ACKNOWLEDGEMENT**

Firstly, all prizes belong to Almighty God who gives us life, strength, and time as well as opportunity to finish this master's thesis. Secondly, I would thank to my supervisor, Prof. Jong-Soo Lee, co-advisor, Dr. Younghoon Kim, and the committee member, Prof. Youngu Lee for the great guidance so far. I want to thank my family members for all the motivations and emotional supports whenever I needed. A huge respect and appreciation go for my great labmate, Min-Hye Jeong, who contribute a lot to my works. I also want to thank all MNEDL Lab members, Seock-Jin Jeong, Jigeon Kim (student of R3) and also alumnae, Kwak Do-Hyun and Hyun-Soo Ra and Na-Yeon Kim. A great appreciation also goes to all my Indian family in DGIST, for the companion. Lastly, all thanks to my Korean and Foreigner friends who I can not mention all the names. Much success will come.